NJC

Accepted Manuscript

This article can be cited before page numbers have been issued, to do this please use: S. Mondal, T. Rajesh, B. B. Dhar, M. Snellman, J. Li, L. D. Francis and R. N. Devi, *New J. Chem.*, 2017, DOI: 10.1039/C7NJ03652C.

ROYAL SOCIETY OF CHEMISTRY

rsc.li/njc

View Article Online
DOI: 10.1039/C7NJ03652C

Journal Name

ARTICLE

Understanding alloy structure and composition in sinter-resistant AgPd@SiO_2 encapsulated catalysts and their effect on catalytic properties

Received 00th January 20xx,
Accepted 00th January 20xx

DOI: 10.1039/x0xx00000x

www.rsc.org/

Sourik Mondal,[a] Thattarathody Rajesh,[a] Basab B Dhar,[b] Markus Snellman,[c] Junjie Li,[c] Francis Leonard Deepak,*[,c] R. Nandini Devi,*[,a]

Extent of alloying and alloy composition, crucial in determining the activity and selectivity of bimetallic catalysts, are studied in porous silica encapsulated AgPd catalysts using XRD, HRTEM and HAADF-STEM. Water dispersible ligand protected Pd ultra small clusters and Ag nanoparticles of three different sizes are used as precursors. High reactivity of Pd ultra small clusters enhances alloying of even big Ag nanoparticles to an extent. Encapsulation seems to have minimised the sintering of the resultant nanoparticles. Earlier suggestions of role of d-band positions with respect to adsorption energies holds good for AgPd system also and alloying enhances the activity. Alloy of composition Ag50Pd50 is found to be the most active with rate of the reaction enhanced two fold in this system compared to other compositions. Other factors like particle size and sinter-resistance also play important roles in enhancing the activity of these catalysts.

Introduction

Catalysis on bimetallic systems has been under focus for their advantage of the synergistic effect of various properties of the pure component metals.[1-3] Geometric and electronic factors like ensemble effect and ligand effect are suggested to play an important role in this.[1] Ensemble effect has a geometric origin in which particular arrangements of atoms on the metal surface assist a specific catalytic process, whereas ligand effect is electronic in nature arising out of electron transfers between the heteroatoms in the bimetallic systems. Even though attempts have been made to explain the catalyst properties based on either of these characteristics, a cooperative effect possibly manifests here. Primary markers for efficient catalysis, like ease of reactant adsorption and product desorption from alloy surface and attendant activation energies can be affected by both electronic and geometric effects. Knowledge of adsorption energies and d-band centres can also help in aligning the right elements for maximising the activities and selectivities.[4-7] For instance, mixing a metal with strong binding characteristics to a metal which has high barrier for binding is shown to give optimal results. A combination of Ag and Pd is proposed to be a good candidate for various industrially important reactions like formic acid dehydrogenation,[8] methyl acrylate hydrogenation,[9] ethanol oxidation,[10] oxygen reduction reaction[11] etc., since Ag and Pd has the most disparate d-band centers.

p-nitrophenol (PNP) reduction using $NaBH_4$ is a well known reaction, suggested to be a good probe for studying structural and kinetic aspects due to its simplicity and clean product distribution. Catalysts ranging from metal nanoparticles to metal oxides on various supports are studied for this reaction.[12,13] This would be appropriate in case of understanding AgPd alloy systems, since the PNP molecule is observed to bind weakly to Ag and quite strongly to Pd.[14] Geometric effect may manifest in the alloy particle size as well as extent of alloying which in turn depends on the synthesis method, heat treatment, extent of sintering etc. It is now obvious that the alloy surface properties vis-a-vis structure as well as composition can be correlated to the catalytic activity. Hence understanding the electronic effects and optimising the alloy composition and developing new synthetic methods etc. are of utmost importance.

Most of the earlier reported works in AgPd based catalysts exist in the premise of colloidal nanoparticles synthesised by using protecting ligands.[15-17]For more practical applications in heterogeneous catalysis, it is imperative to have well dispersed nanoparticles stabilised on supports. Most widely used catalyst design is that of metal nanoparticles dispersed on support surface synthesised by simple methods like

[a] Catalysis and Inorganic Chemistry Division
CSIR-National Chemical Laboratory
Dr. Homi Bhabha Road, Pune 411008, India
E-mail: nr.devi@ncl.res.in
[b] Chemical Engineering and Process Development Division
CSIR-National Chemical Laboratory
Dr. Homi Bhabha Road, Pune 411008, India
[c] Department of Advanced Electron Microscopy, Imaging and Spectroscopy,
International Iberian Nanotechnology Laboratory, Avenida Mestre Jose Veiga,
Braga 4715-310, Portugal

Electronic Supplementary Information (ESI) available: [details of any supplementary information available should be included here]. See DOI: 10.1039/x0xx00000x

View Article Online
DOI: 10.1039/C7NJ03652C

impregnation using precursor salts followed by appropriate heat treatments. Recently, the technique of dispersion of pre-synthesied AgPd nano-alloys on carbon support have been used for electrochemical applications.[18] Fabrication of AgPd nanorings supported on graphene nanosheets also have been achieved by galvanic displacement strategy between the Pd ions and pre-synthesised Ag nanoparticles.[19] Similar strategy was followed for the synthesis of Ag-Pd nanotubes which showed high electrocatalytic activity for formic acid oxidation.[20]

Even though widely used, such methods are plagued with problems of wide range of particle sizes, sintering at harsh reaction conditions and consequent deactivation etc.[21,22] In this context, we have developed a novel synthesis method in which arrays of ammonium ended thiolate protected water dispersible ultra-small nanoclusters of metals are encapsulated completely within silica spheres. The advantage of this method is that encapsulation within the oxide matrix minimises sintering under drastic conditions. Moreover, abundant organics in the clusters act as template providing porous structure to the silica matrix on their removal, facilitating access of reactant molecules to the active metal surfaces. This has also been observed to enhance alloying at higher temperatures without leading to sintering and segregation.

In this paper, we report a systematic study of synthesis of Ag-Pd bimetallic silica encapsulated catalysts from ultra-small Pd clusters and Ag nanoparticles of various sizes with the aim of identifying the evolution of the bimetallic phases and the effect of Pd and Ag concentration and size on alloying. Ag has more propensity to sinter than Pd due to its low Tamman temperature[23] and hence the stabilising effect of Pd on Ag nanoparticles is also worth studying. We have also attempted at correlating the electronic effect of these variables on catalytic activity based on p-nitrophenol reduction.

Experimental Section

Synthesis. Synthesis and characterisation of the ligand N,N,N-Tripropyl(11-mercaptoundecyl)ammonium Chloride and Pd and Ag ultra-small nanoclusters are reported elsewhere.[24-26] Typically the Ag nanoparticles are synthesised by using low concentration of the ligand as that used in the synthesis of nanoclusters in presence of a strong reducing agent like $NaBH_4$ at room temperature in aqueous medium. The nanoparticle solution is then dialysed to remove the excess reactants present in the solution and final solution is then stored at 4^{o}C. Based on the concentration of thiol used, silver nanoparticles of varying particle sizes are formed, i.e., big nanoparticles (b-AgNPs), medium sized nanoparticles (m-AgNPs) and small nanoparticles or nanoclusters (s-AgNPs). The bimetallic encapsulated samples are synthesised by previously reported hydrolysis and silica condensation method. 10 mL mixture of each of the b-Ag NPs (1.6mM), m-AgNPs (1.6mM) and s-AgNPs (1.6 mM) with Pdnanoclusters (1.7 mM) in the atomic ratio 1:1 were sonicated for 1 h. To each of the sonicated solutions (10 mL), 0.1 M NaOH solution (0.9 mL) was added followed by addition of 0.3 mL tetraethyl orthosilicate (TEOS). This mixture was then vigorously stirred at 25 ^{o}C for 3 days. Silica encapsulated Ag-Pdnanoclusters and nanoparticles were separated from the reaction medium by centrifugation at 14,000 rpm and redispersed in water several times. The as-synthesised samples were dried at 80 ^{o}C for 1 day. In-situ powder x-ray diffraction of the as-synthesised samples wascarried out under air, Ar and 5% H_2/N_2. Each of the samples was calcined at 300 ^{o}C for 1 h to remove the organics, thereby facilitating alloying. Reduction was performed at this temperature for 1 h and further heated to 400^{o}C under H_2 atmosphere and kept at that temperature for 1 h and finally slowly cooled to 30 ^{o}C. In each step the ramping rate was fixed at 5 ^{o}C min^{-1}.

Bimetallic samples supported on silica were synthesised by impregnation method. For this, 5 wt % of Ag-Pd on SiO_2 was prepared by mixing each of solutions of b-AgNPs (7.6 mL, 1.6 mM), m-AgNPs (7.6 mL,1.6 mM) and s-AgNPs (7.6 mL,1.6 mM) with Pd nanoclusters (6.8 mL, 1.7 mM) respectively followed by sonication for 1 h. To each of these solutions, silica nanopowder (particle size of 10-20 nm, Aldrich) was added and this mixture was stirred vigorously at 28 ^{o}C for 1 day. The final solid product was obtained by removing the solvent in vacuum at 80 ^{o}C. This material was then calcined at 300 ^{o}C for 1 h to remove the organics. This calcined material was then further heated to 400 ^{o}C under H_2 atmosphere and kept at that temperature for 1 h and then cooled to room temperature.

Characterisation. UV-Vis spectrophotometry (Cary5000 UV-Vis-NIR spectrophotometer) was used to characterise the silver nanoparticles and nanoclusters, palladium nanoclusters and the silica encapsulated material in aqueous medium. UV-Vis spectra were measured by using quartz cuvettes of 10 mm path length of volume 2 mL. The amounts of silver and palladium in the nanoparticle solutions were estimated by inductively coupled plasma atomic emission spectroscopy on Spectro Akos, FHS-12. The silver nanoparticle and palladium nanocluster solutions were calcined at 350 ^{o}C for 9 h and the residual material were dissolved in conc. HNO_3 and aqua regia respectively. In case of silica coated samples, elemental analysis was carried out by EDAX on a Scanning Electron Microscope (Leica Stereoscan 440) with EDS attachment (Bruker, D451-10c Energy Dispersive X-ray spectrometer). Powder x-ray diffraction (XRD) of all the samples was carried out in a PANalyticalX'Pert Pro dual goniometer diffractometer working under 40 kV and 30 mA. The radiation used was Cu Kα (1.5418 Å) with a Ni filter and the data collection was carried out using a flat holder in Bragg– Brentano geometry with 1^{o} slit at the source side. An X'celerator solid-state detector with a step size of 0.0084^{o} and time per step of 30.5 s was employed. For powder XRD refinement, data were collected with a step size of 0.0084^{o} and a time per step of 184.785 s. Variable temperature in-situ XRD experiments were carried out in an Anton-Parr XRK 900 reactor under air, argon and 5% H_2/N_2. Powder XRD refinement was done using Rietveld method by means of the GSAS-EXPGUI

View Article Online
DOI: 10.1039/C7NJ03652C

program.[27] Initially background and scale factors were refined followed by cell parameters and profile parameters. FEI Tecnai T-20 electron microscope, operating at 200 kV was used for TEM sample observation. To prepare the specimen for TEM/STEM, the samples were dispersed in ethanol by ultrasonication and a drop of this dispersion was placed on a holey carbon grid and dried. TEM/STEM analysis at both 80 kV and 200 kV was performed on FEI Titan ChemiSTEM equipped with a probe corrector, Super-XEDS detector and Gatan EELS spectrometer. EDS quantification was carried out by employing the Cliff–Lorimer method in Esprit Software.

Results and Discussion

The synthetic strategy followed here is different from the conventional methods where Ag and Pd ions act as precursors. We employ already formed nanoforms as precursors and the formation of bimetallics is expected at high temperatures. This will also help in understanding the sintering phenomenon better as well as the role of initial particle size in this process and the extent of their reactivity can thus be explored. Nanoforms such as nanoparticles and ultra small clusters of Ag and Pd are synthesised using a cationic ammonium headed alkyl thiol ligand specially designed in our laboratory. The ligand structure is such that the thiol group in one end ensures binding to the metal and the ammonium at the other end of the long chain alkyl group makes it water dispersible. Such water dispersible nanoforms have been used for further silica encapsulation by a simple hydrolysis and condensation of a silica precursor like tetraethoxysilane (TEOS). The propyl groups in the quaternary ammonium ions provide a mildly hydrophobic region around the clusters. This region probably presents a conducive interaction to the hydrophobic TEOS leading to silica encapsulation of individual clusters within the silica sphere, even though they are present in arrays. In this way, a core shell model with all the clusters in the core with a nonporous silica shell can be prevented. This, to a large extent, helps in minimising sintering which is proposed to occur due to the coalescence of smaller particles on the support surfaces. This method has previously been successfully utilized for Au, Pd, Ag nanoclusters and their bimetallic systems.[24-26] In the present work, we selected Ag nanoparticles (NP) with three different particle sizes and reacted with Pd ultra small clusters of size below 2 nm, mainly to understand the effect of Ag NP size and reactivity on the formation of AgPd bimetallic systems. Ag:Pd molar ratio in the synthesis mixture was kept constant at 1:1 (Scheme 1).

It is known that sizes of metal nanoparticles can be changed by varying the concentration of the capping agents like thiol. In case of Ag, three different particle size ranges were synthesised using Ag:thiol molar ratios of 1:0.12, 1:2 and 1:4. The variation in particle size could be unambiguously evidenced from UV-Vis spectroscopy through surface plasmon resonance (SPR) peaks (Supporting Information S1).

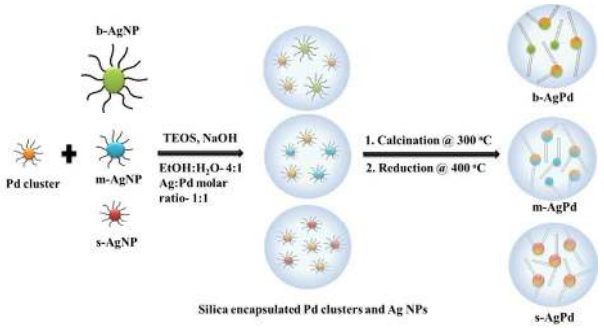

Scheme 1 Schematic representation of the synthesis of AgPd@SiO_2 catalysts from ultra-smallPdnanoclusters and Ag nanoparticles of three different sizes (s-, m- and b- denoting small, medium and big, distinguished based on their surface resonance plasmon peak characteristics

Ag nanoparticles exhibit SPR characteristics in the visible range around 410 nm for metal nanoparticles of size > 2 nm.[28,29] The UV-Vis spectrum of the Ag thiolate sample (1:0.12 Ag:thiol composition) shows the presence of a strong SPR peak with a maximum at 410 nm. The intensity of this peak reduces to a mere hump and shifts to higher wavelength when the ratio becomes 1:2 indicating sharp decrease in the particle size.[30] At a ratio of 1:4,the SPR peak completely disappears indicating the absence of nanoparticles of sizes above 2 nm. This sample is considered as ultra-small nanocluster which does not show typical metallic nanoparticle properties like SPR. A thorough electron microscopy study on the Ag NPs indicate corroborating results, with progressively decreasing particle sizes as ligand concentration increases. HRTEM images of the Ag nanoparticles of three Ag:thiol ratios (along with histograms) and Pd nanoclusters are given in Supporting Information S2. It is to be noted here that Ag ultra small clusters displayed agglomeration under electron beam and hence big particles are not considered for histogram. A similar conclusion can be derived from powder x-ray diffraction (PXRD) patterns indicating the size differences in the three samples (Supporting Information S3).

Synthesis of encapsulated samples was carried out by simple silica condensation under alkaline conditions. Ag:Pd concentration ratio of 1:1 is employed for all the three Ag particle sizes, big, medium and small. HRTEM images of the as-synthesised materials (Supporting Information S4) show full encapsulation of the nanoparticles and nanoclusters. Final catalysts are obtained by calcining these materials at 300 °C and further reduction at 400 °C. For the sake of clarity, the samples are differentiated based on Ag particle sizes as s-, m-, and b- denoting small, medium and big Ag NPs. For comparison, pure Ag and Pd encapsulated in silica also were synthesised and analysed. The metal concentrations initially added for the synthesis as well as analysed by EDAX are correlated and indicates good incorporation of the metals into the silica matrix in the final samples (Supporting Information S5).

View Article Online
DOI: 10.1039/C7NJ03652C
ARTICLE Journal Name

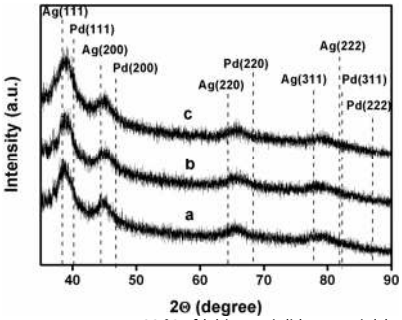

Fig. 1. Powder XRD patterns at 400 °C of (a) b-AgPd (b) m-AgPd (c) s-AgPd.

A comparative plot of the XRD patterns of the three samples at 400 °C under H_2 is shown in Fig. 1 and evidence of the presence of metallic phases is seen from the intense peak corresponding to (111) plane of Ag or Pd. In case of s-AgPd the (111) peak corresponds to pure alloy phase only, when compared to m-AgPd and b-AgPd which contain multimodal peaks corresponding to alloy phase and Ag phase. This is also corroborated by UV-Vis spectra of the as-synthesised and calcined-reduced samples (Supporting Information S6). It is known that alloying with metals like Pd which does not display SPR peaks masks such characteristics in metals like Au, Ag etc.[31,26] Indeed we observe the same phenomenon further proving alloying to a large extent.

Table 1. Rietveld parameters of the catalysts*

Parameters	s-AgPd	m-AgPd	b-AgPd
χ^2	0.94	1.085	0.78
wRp (%)	1.63	1.79	6.99
Rp (%)	1.29	1.41	5.50
a(Ag) (Å)	0	4.0860(4)	4.0868(18)
a(AgPd) (Å)	4.0201(3)	3.9877(6)	4.0052(16)
a(Pd) (Å)	0	0	0
V(AgPd)	64.971(15)	63.412(26)	64.248(79)
Wt% (Ag)	0	19	38
Wt%(AgPd)	100	81	62
Wt% (Pd)	0	0	0
Percentage composition (%)	alloy 100	alloy Ag 81 19	alloy Ag 62 38

*χ^2: Goodness of fit,$\chi 2 = M/(Nobs - Nvar)$ where M=Minimization function, N_{obs}=total number of observations in all histograms and N_{var}= number of variables in the least squares refinement; Rp: Profile Factor, $Rp = (\sum|Io - Ic|) / (\sum Io)$ where Io and Ic are the observed and calculated integrated intensities; wRp: Weighted Profile Factor, $wRp=\sqrt{Mp/\sum wIo^2}$ where Mp=minimization function for the powder diffraction data.

A systematic Rietveld refinement of the patterns further reveals an interesting trend in the evolution of the bimetallic system and extent of alloying (Table 1; refinement plots are given in Supporting Information S7). In s-AgPd, only one metallic phase is present with cell parameter deviating more towards Ag indicating a slightly Ag rich alloy. But in m-AgPd and b-AgPd samples, two metallic phases (pure Ag and alloy) can be identified. In addition, the extent of alloying is found to be higher in case of samples synthesized from medium Ag particles compared to big Ag particles, as is evident from the quantitative phase analysis results.

TEM images of the three samples give an overall picture of the particle sizes and extent of sintering. Fig. 2 displays the TEM images and particle size histograms of the encapsulated catalysts in comparison with surface supported cluster samples, both sets heated to 400 °C.

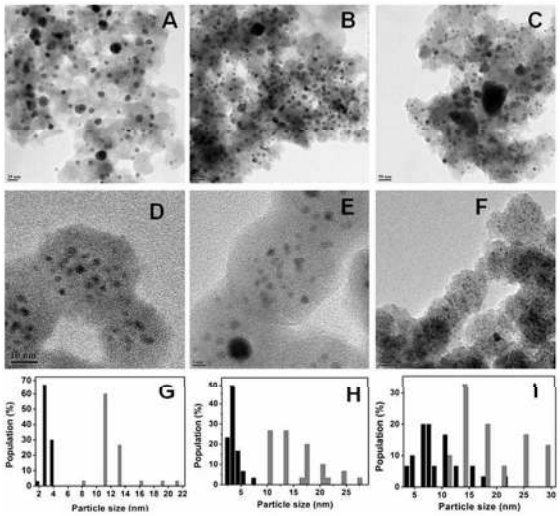

Fig. 2 TEM images of surface supported samples s-AgPd, m-AgPd and b-AgPd (A,B,C respectively) and their corresponding encapsulated samples (D,E,F respectively). The histograms of the corresponding surface supported samples (grey) and encapsulated ones (black) are represented by G,H and I. Scale bars = 20 nm (A), 50 nm (B), 50 nm (C), 10 nm (D), 5 nm (E), 20 nm (F).

It is obvious that sintering is highly controlled in the encapsulated samples, especially in case of s- AgPd@SiO_2. Average particle size of the s-AgPd alloy was found to be 3 nm and this increased to 4 nm in case of m-AgPd and 10 nm in b-AgPd. Dispersity of the particles is also controlled better in s-AgPd (2-4 nm) than the other two (2-7 nm in m-AgPd and 2-17 nm in b-AgPd). The average particle size of the surface supported catalysts is shifted to higher values in all the three cases. Interestingly, here the average particle size seems to be more or less same in all three samples irrespective of the Ag precursor size indicating uncontrolled coalescence mechanism in play here. This is controlled in the encapsulated samples even when big Ag precursor particles are used.

At this stage it is imperative to shed more light on the structure and composition of the alloy nanoparticles for

View Article Online
DOI: 10.1039/C7NJ03652C

further understanding the mechanism of alloy formation and correlation to catalytic properties. For this, a thorough lattice fringe analysis by high resolution transmission electron microscopy (HRTEM) and subsequent Vegard's law fit was carried out in multiple particles (Detailed explanation and data given in Supporting Information S8). Representative images are shown in the panels in Fig. 3.

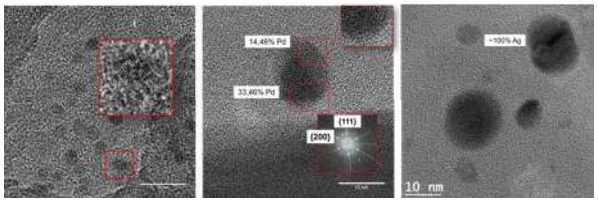

Fig. 3 HRTEM images and lattice fringe analysis of (left) s-AgPd, (middle) m-AgPd and (right) b-AgPd. Inset shows highly crystalline pure alloy phase (s-AgPd), segregated Pd phase of comparable composition (m-AgPd) and pure Ag phase (b-AgPd) in a single particle domain. Scale: 10 nm

In s-AgPd, each particle analysed is uniform in composition and shows appreciable extent of alloying. However, in case of m-AgPd, non-uniform particles start to appear. In this system, regions of different composition exist within the same particle. For instance, two different compositions of 14 and 33% Pd are detected in the same alloy particle. This effect gets more severe in case of b-AgPd and pure Ag particles without Pd or very small concentrations of Pd (5-10%) are seen. Most importantly, the particles when alloyed seem to have more or less similar compositions (30-60% Pd) in both the cases. These observations corroborate those from XRD, which indicate pure Ag particles in m- and b-AgPd samples. Another interesting observation from HRTEM was the presence of twinned and interfacial particles in m- and b-AgPd samples (Supporting Information S9) which arises due to the slow reaction kinetics of bigger Ag particles.

Further, a detailed elemental analysis of individual particles by high-angle annular-dark-field scanning TEM (HAADF-STEM) images throws more light on the mechanistic aspects of the reaction between the particles (Supporting information S10). Representative images are shown in Figure 4.

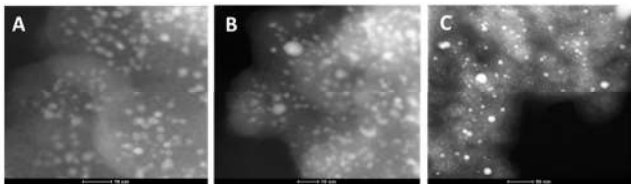

Fig. 4 HAADF-STEM images of s-AgPd (A), m-AgPd (B) and b-AgPd(C). Scale bar: 10 nm (A), 10 nm (B), 50 nm (C).

In the outset, the data corroborates our observations from other techniques that particle size is highly controlled and more uniform in case of s-AgPd whereas sintering is more severe in case of the other two indicating the role of precursor particle size and their reactivity in defining the final particle size. Elemental analysis and mapping is given in Fig. 5 (detailed images are given in Supporting Information S11). s-AgPd shows an intimate mixing of Ag and Pd as clear from the mapping. Quantification of the metal concentrations give Ag:Pd atomic % ratio of ~50:50. In case of m-AgPd, clearly dispersity is affected and segregation of pure Ag phase is observed. For instance, in the representative image given in Fig.5, panel B, particles of Ag are clearly visible (white dotted circles in panel E).

The alloy particles show higher concentrations of Ag (Ag69Pd31) when compared to s-AgPd. Portions with higher concentrations of Ag also could be seen in abundance. Similar observation can be made in case of b-AgPd. Here, more number of unalloyed Ag particles is present and alloy particles are enriched in Ag (Ag64Pd36) as in case of m-AgPd. It becomes apparent that even bigger Ag particles are reactive towards alloying in the temperature range in this study. Looking closely at the interfaces of Ag only portions (as intimated by the dotted circles in Fig. 5), it is evident that Pd ultra small clusters may be imparting the reactivity to bigger Ag nanoparticles. It is possible that at higher temperatures or longer durations of heat treatment, better alloying can be attained. It is noteworthy here that such treatments are possible and better alloying attained in the encapsulated samples since in conventional catalysts, severe sintering is observed. This shows the advantages of the present method by which already formed Ag nanoparticles prone to sintering can be made not only reactive for alloy formation but also resistant to sintering.

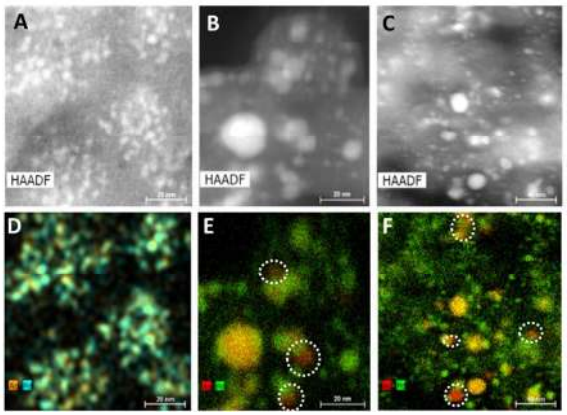

Fig. 5 HAADF images and elemental mapping in the catalysts. Ag and Pd distribution are represented by yellow and blue respectively in panel D, red and green respectively in panels E&F). White dotted circles highlight the segregation of Ag phase from Pd in case of m-AgPd and b-AgPd. Scale: 20 nm (A-F).

p-Nitrophenol (PNP) reduction was used as a reaction probe to understand the alloy structure further. Catalyst amounts were taken by fixing the total metal concentration so that activities can be compared. The UV-Vis spectra of the reaction mixture were collected at regular intervals as given in Supporting Information S12. 0.2 M $NaBH_4$ solution in water (750 µL) was added to 80 mM solution of PNP in water (250 µL) with constant stirring. 25 µL of catalyst solution prepared by dispersing 1 mg of the catalysts (s-AgPd and m-AgPd) and

View Article Online
DOI: 10.1039/C7NJ03652C

1.4 mg (b-AgPd) in 1 mL water was added to the above solution. Aliquots of this solution were used from time to time for recording the UV-Vis spectra. All the experiments were done at 20 ^{o}C. The absorption spectra of PNP show an intense peak at 400 nm. The intensity of this band gradually reduces and another band appears at 300 nm characteristic of p-aminophenol due to the reduction of NO_2 group to NH_2. It was observed that complete decolourisation of the bright yellow coloured solution of p-nitrophenol by s-AgPd occurred after 45 min, which is faster as compared to other catalysts of same concentration. A detailed kinetic analysis was carried out to arrive at the variations in rates of the reaction for all the catalysts, using UV–vis spectroscopy at λmax of p-nitrophenol (400 nm) under pseudo-first- order conditions. The pseudo first-order rate constant (kobs) calculated from the absorbance vs time traces were obtained from nonlinear curve fitting [(At= Aα– (Aα– Ao)e(-kobs t)]. The time course graph for the conversion of PNP to p-aminophenol (PAP) is shown in Fig. 6. A comparison of the ease of decolourisation which gives an insight into the rate of the PNP reduction based on the concentration of unreacted PNP (initial concentration of 80 mM) after 45 min is given in the inset of the same figure.

It shows that as Ag particle size increases, rate decreases and as a result concentration of PNP left unreacted after 45 min gradually increases from s-AgPd to m-AgPd to b-AgPd. It is worth noting here that the surface supported catalysts (s-AgPd/SiO_2) showed very poor activity and full decolourisation was not observed even after 7 h.

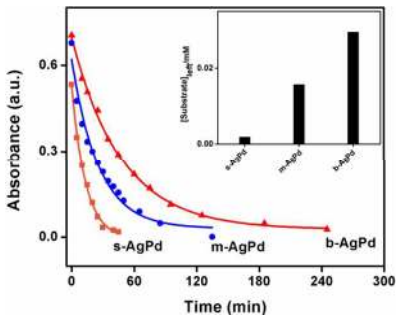

Fig. 6 Time course graph for the conversion of PNP to PAP by s-AgPd, m-AgPd and b-AgPd. Inset bar graph shows the concentration of unreacted PNP after 45 min.

The rates of the reaction with respect to the alloy composition are given in Supporting Information S13, from which it is clear that the rate of the reaction on s-AgPd is the highest, at least twice that of pure Ag and Pd catalysts. Highly Ag rich alloys are comparatively less active. In addition, the activity is clearly affected by the particle sizes and extent of dispersity which is found to be better for samples synthesised from small Ag particles. Recyclability of a selected catalyst s-AgPd was tested for three cycles and the activity was found to be comparable to the activity of fresh catalyst of the same quantity (Supporting Information S14).

Correlating alloy composition and particle size to catalytic activity throws up some interesting observations (Fig. 7). Confluence of controlled particle size, large extent of alloying and appropriate alloy composition has placed s-AgPd advantageously in terms of catalytic activity. Random yet intimate mixing of Ag and Pd devoid of contiguous islands of single composition in s-AgPd suggests that ligand effect which is electronic in nature may predominate the activity. Rather interesting is the comparison between m- and b-AgPd which have similar alloy composition and particle size, yet different activities. The difference in characteristics to be noted here is the extent of alloying, which is much higher for m-AgPd (80:20 alloy:Ag) compared to b-AgPd (60:40 alloy:Ag). The alloy composition enriched in Ag (Ag69Pd31 and Ag64Pd36 for m- and b-AgPd respectively) also indicates contiguous Ag islands in these nanoparticles. From the catalytic activity data, it is clear that Ag is poor in activating PNP; hence Ag rich surface is obviously detrimental for PNP reduction activity. Ag rich nanoparticles, in addition to higher concentration of unalloyed Ag particles, make b-AgPd least active in the set of three catalysts studied here. The fact that s-AgPd average particle size is not hugely different from the other two samples also indicates a bigger role played by alloy composition and ligand effect.

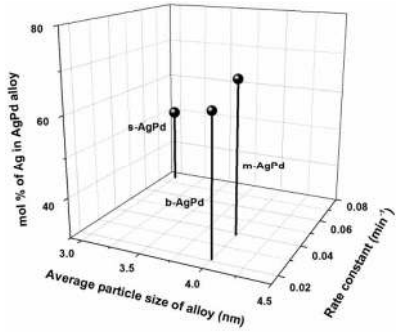

Fig.7 Mapping of three catalysts in terms of average alloy particle size, rate constants and mol % of Ag in the alloy.

Conclusions

Extensive studies on bimetallic systems have revealed the effect of composition manifesting as a dilution effect of strongly binding metal with less reactive metal by which contiguous ensembles of the former are created. As the concentration of the weakly binding metal increases, these ensembles become islands and eventually form isolated atoms, named as ensemble effect. Another parameter which starts playing an important role in intimately mixed alloys is the ligand effect in which advantageous electron transfers between the individual atoms of the bimetallics occur. These cooperative effects balancing weak and strong binding of constituent metals, when optimised lead to the best bimetallic catalysts. In the set of three silica encapsulated AgPd alloy catalysts studied in this work, s-AgPd (synthesized from Ag and Pd ultra small clusters) with 50:50 alloy

View Article Online
DOI: 10.1039/C7NJ03652C

composition and intimate mixing of constituent atoms devoid of contiguous islands show the best activity in para-nitrophenol reduction, which may indicate a bigger role of ligand effect. The other two catalysts, m- and b-AgPd, with similar average particle size and composition (Ag69Pd31 and Ag64Pd36) also differ in their activity due to variation in extent of alloying (20 and 40 wt% unalloyed Ag respectively). Hence, this study takes into consideration three important parametric markers, particle size, extent of alloying and alloy composition and has identified the best catalytic system. By avoiding sintering effect, the encapsulation method can also enhance the activity and durability of nanocatalysts.

Acknowledgements

Authors acknowledge the financial help from NWP56 project under the TAPSUN programme funded by CSIR and the authors thank Dr. E. A. Anumol for useful discussions. MS, JJL and FLD acknowledges the financial support provided by NORTE 2020 through the European Regional Development Fund (ERDF).

References

1 V. Mazumder, M. Chi, M. N. Mankin, Yi. Liu, O. Metin, D. Sun, K. L. More and S. Sun, *Nano Lett.,* 2012, **12**, 1102-1106.
2 D. A. Slanac, W. G. Hardin, K. P. Johnston and K. J. Stevenson, *J. Am. Chem. Soc.,* 2012, **134**, 9812-9819.
3 A. K. Singh and Q. Xu, *Chem. Cat. Chem.*, 2013, **5**, 652–676.
4 B. Hammer and J. K. Nørskov, *Nature*, 1995, **376**, 238–240.
5 B. Hammer, Y. Morikawa and J. K. Nørskov, *Phys. Rev. Lett.*, 1996, **76**, 2141–2144.
6 B. Hammer and J. K. Nørskov, *Surf. Sci.* 1995, **343**, 211–220.
7 B. Hammer, *Top. Catal.,* 2006, **37**, 3–16.
8 S. Zhang, O. Metin, D. Su and S. Sun, *Angew. Chem. Int. Ed.,* 2013, **52**, 3681-3684
9 J. H. He, I. Ichinose, T. Kunitake, A. Nakao, Y. Shiraishi and N. Toshima, *J. Am. Chem. Soc.*, 2003,**125**, 11034–11040.
10 G. Li, L. Jiang, Q. Jiang, S. Wang and G. Sun, *Electrochim. Acta*, 2011, **56**, 7703 –7711.
11 W. Tang and G. Henkelman, *J. Chem. Phys.*, 2009, **130**, 194504.
12 C. Du, S. He, X. Gao and W. Chen, *Chem. Cat. Chem*, 2016, **8**, 2885-2889
13 C. Zhang, R. Zhang, S. He, L. Li, X. Wang, M. Liu and W. Chen, *Chem. Cat. Chem.*, 2017, **9**, 980-986
14 Z. D. Pozun, S. E. Rodenbusch, E. Keller, K. Tran,W. Tang, K. J. Stevenson and G.Henkelman, *J. Phys. Chem. C*, 2013, **117**, 7598−7604.
15 Y. Lu and W. Chen, *ACS Catal.*, 2012, **2**, 84−90.
16 H. Rong, S. Cai, Z. Niu and Y. Li, *ACS Catal.*, 2013, **3**, 1560−1563.
17 D. Sun, P. Li, B. Yang, Y. Xu, J. Huang and Q. Li, *RSC Adv.,* 2016, **6**, 105940-105947.
18 Y. Lu, Y. Jiang, X. Gao, X. wang and W. Chen, *Part. Part. Syst. Charact.* 2016, **33**, 560–568.
19 M. Liu, Y. Lu and W. Chen, *Adv. Funct. Mater.*, 2013, **23**, 1289-1296.
20 Y. Lu and W. Chen, *J. Phys. Chem, C*, 2010, **114**, 21190-21200.
21 R. S.Goeke and A. K. Datye, *Top.Catal.,* 2007, **46**, 3–9.
22 J. Matos, L. K. Ono, F. Behafarid, J. R. Croy, S. Mostafa, A. T. DeLaRiva,A. K.Datye,A. I.Frenkel and B. R. Cuenya, *Phys. Chem.Chem. Phys.,* 2012, **14**, 11457–11467.
23 S. E. Golunski, *Platinum Metals Rev.* 2007, **51**, 162.
24 A. Samanta, B. B. Dhar and R. N. Devi, *J. Phys. Chem. C,* 2012, **116**, 1748– 1754.
25 A. Samanta and R. N. Devi, *Chem. Cat. Chem.,* 2013, **5**, 1911–1916.
26 S.Mondal, A.Samanta,B. B. Dhar and R. N.Devi, *Catal.Today,*2015,**25**, 114-120.
27 B. H. Toby, *Appl. Crystallogr.,* 2001, **34**, 210-213.
28 S. Link and M. A. Sayed, *Int. Rev. Phys. Chem.,* 2000, **19**, 409-453.
29 C. A. J. Lin, C. H. Lee, J. T. Hsieh, H. H. Wang, J. K. Li, J. L. Shen, W. H. Chan, H. I. Yeh and W. H. Chang, *J. Med. Biol. Eng.*, 2009,**29**, 276-283.
30 S. Peng, J. M. McMahon, G. C. Schatz, S. K. Gray and Y. Sun, *PNAS*, 2010, **107**, 14530-14534.
31 A. Samanta, T. Rajesh and R.N. Devi, *J. Mater. Chem. A*, 2014, **2**, 4398-4408.

View Article Online
DOI: 10.1039/C7NJ03652C

Table of content entry:

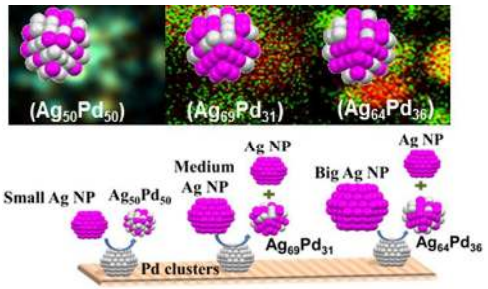

Effect of precursor particle size, extent of alloying and alloy composition in $AgPd@SiO_2$ catalysts